J Electroceram (2014) 32:319–323
DOI 10.1007/s10832-014-9902-8

Parabolic behavior of solution processed ZnSnO device performances depending on Zn/Sn ratios

Hye-Ji Jeon · Kwun-Bum Chung · Jin-Seong Park

Received: 20 January 2014 / Accepted: 4 February 2014 / Published online: 26 February 2014

Abstract Thin film transistors (TFTs) with amorphous zinc tin oxide (ZTO) channel layer were fabricated by a simple and low-cost solution process, prepared by dissolving 0.2 M of zinc acetate dihydrate and tin chloride dihydrate in 20 mL of 2-methoxyethanol. All ZTO thin films showed amorphous phases and no impurities (no carbon and chlorine content) even at process temperature of 350 °C. As the Sn ratio in ZTO films increased, the values of saturated mobility (u_{sat}) and subthreshold gate swing (SS) exhibited a parabolic behavior in ZTO TFTs, depicting that the μ_{sat} and SS values were a maximum (3.4 cm^2/V.s) and minimum (0.38 V/decade) at Zn/Sn=1 ratio. Interestingly, the x-ray absorption and X-ray photoemission spectroscopy revealed the origin of parabolic behavior, indicating not only to improve a charge transport in conduction bands but also to increase the Sn^{4+}/Sn^{2+} ratio at the peak values (Sn/(Zn+Sn)=1).

Keywords Thin film transistor · Oxide semiconductor · Solution process

1 Introduction

In early 2013, LG display has launched commercial 55-in active matrix organic light emitting diode (AMOLED) television in the world. Remarkably, the amorphous oxide semiconductors (AOS) material was adopted as a channel layer in the AMOLED TV. Since 2004, amorphous oxide semiconductor thin film transistors (AOS-TFTs) have been interested as potential switching devices for active matrix display applications, because of their superior performance, which typically exhibit field effect mobility values of over 10 cm^2/Vs. In addition, the major advantage of AOS materials is that they can be deposited using conventional semiconductor process methods such as sputtering at room temperature, and their amorphous structures enable the realization of uniform device properties on large areas [1, 2].

Mostly, AOS materials have been prepared by vacuum processes such as physical vapor deposition (PVD) methods, which require expensive equipment and high fabrication costs [3, 4]. Unfortunately, this process may be a potential obstacle for its use in low-cost large-area electronics. So, the formation of amorphous oxide TFTs was intensively investigated by using solution-based methods, which offer great benefits such as the simplicity, low cost, and high throughput. Recently, various precursor based spin-coating process can be considered to be one of the best available processes for large area fabrications [5–7]. Among various solution processed oxide semiconductors, indium-free based oxide materials such as aluminum zinc tin oxide [8], gallium zinc oxide [9], and zinc tin oxide (ZTO) [10] have been reported as channel layers because of their low costs and easy processes. Very recently, solution based ZTO materials have been significantly examined for active channel layer for TFTs and achieved high mobility. However, many groups focused to report various metal doped ZTO systems and their electrical performance themselves [11]. There are rarely systematic investigations between device properties and Zn/Sn composition ratio in solution processes.

In this paper, solution precursor based ZTO TFTs fabricated at 350 °C annealing and investigated systematically depending on various Zn/Sn ratios in ZTO films. All ZTO films exhibited amorphous structures upto 500 °C annealing temperature and had no carbon and chlorine impurities even at

H.-J. Jeon · J.-S. Park (✉)
Division of Materials Science and Engineering, Hanyang University, Seoul 133-719, South Korea
e-mail: jsparklime@hanyang.ac.kr

K.-B. Chung
Department of Physics, Dongguk University, Seoul 100-715, South Korea

350 °C annealing. Interestingly, ZTO TFTs showed the parabolic behavior, having maximum mobility value and minimum subthreshold gate swing values on Zn/Sn ratios. The physical and chemical analyses such as X-ray absorption and X-ray photoelectron spectroscopy (XAS and XPS) will reveal the origin of parabolic behavior of ZTO TFT performance.

2 Experiment

The precursor solution was prepared by dissolving a total of 0.2 M zinc acetate dihydrate (Zn-(CH_3COO)·$2H_2O$) and tin chloride dihydrate ($SnCl_2 \cdot 2H_2O$) in 20 mL of 2-methoxyethanol ($CH_3OCH_2CH_2OH$). The chemical composition ratios of ZTO precursor solution were varied with molar ratio of Zn:Sn=10:0, 8:2, 5:5, 2:8 and 0:10. All prepared solutions were stirred to ensure a complete mixture of the solution in a glass vial for 12 h at 60 °C and filtered through a membrane with 0.2 μm pores before being spin-coated. Heavily boron doped silicon substrate with a thermally grown SiO_2 layer was used as a gate and gate-insulator layer, respectively. The substrates were treated by ozone for 20 min, to enhance the coating properties before coating the active layer. The ZTO solution as an active layer was spin coated on the substrate at a speed of 3000 rpm for 30 s. Then, ZTO film was dried at 120 °C for 5 min to evaporate the solvent and annealed at 350 °C for 1 h in air. This fabricated thin film is used as an active channel layer. Aluminum drain and source electrodes having a width (W) of 1000 μm and a length (L) of 150 μm were deposited through a fine metal mask (FMM).

The coating solution was examined via a thermogravimetric analysis (TGA) and differential scanning calorimetry (DSC) under air gas flow and a 10 °C/min heating rate. The film composition was obtained by using Auger electron spectroscopy (AES). The physical and electronic structures of the ZnSnO films were observed using X-ray diffraction (XRD) and x-ray absorption spectroscopy (XAS). The XAS measurements were performed using coherent x-ray beams at the Pohang accelerator laboratory on beamline 7B1. The electrical properties of the TFT devices were measured using a HP4155B analyzer. Finally, the chemical bonding states were examined using X-ray photoelectron spectroscopy (XPS) with a monochromatic MgKα (1253.6 eV) source with a pass energy of 50 eV.

3 Results and discussion

Figure 1(a) shows the thermal behavior of ZTO solution with the ratio of Zn:Sn=1:1, determined by TG/DSC analyses. The TG/DSC analyses exhibited identical thermal behaviors with 3 steps. First, a sharp drop has been occurred below 150 °C. This abrupt weight loss was caused by the evaporation of ZTO precursor solvent, which has a boiling point of 124–125 °C. Second, the weight loss observed above 150 °C represents the thermal decomposition of metal acetates one of the organic group. Finally, $SnCl_2$ related precursors would start to decompose after 350 °C. In previous report [12], thermal behavior analysis of the ZTO solutions (Zinc acetate dehydrate and tin acetate) exhibited thermal decomposition of both the complex ligands associated with the metal acetates above 200 °C.

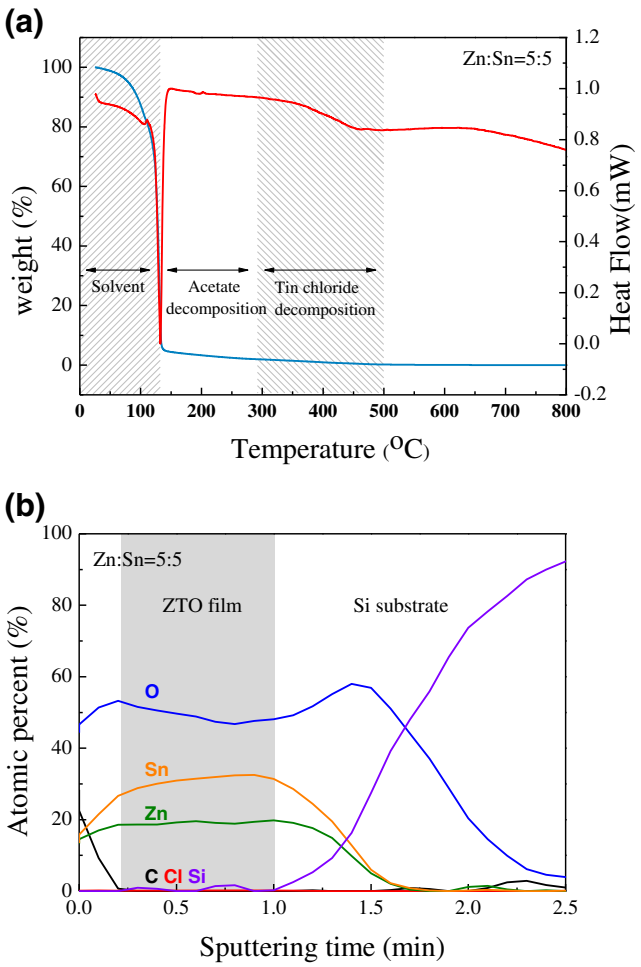

Fig. 1 (**a**) TGA and DSC curves of ZTO precursor material. The Zn: Sn ratio of ZTO precursor is 1:1. (**b**) AES depth profile of the ZTO film annealed at 350 °C (Sn/(Zn:Sn)=1)

Table 1 Summary of elemental composition in various ZTO films

Zn:Sn ratio	Atomic percent (%)				
	Zn	Sn	O	Zn/(Zn+Sn)	Sn/(Zn+Sn)
10:0	33.30	0.00	49.70	1.00	0.00
8:2	21.20	6.20	50.00	0.77	0.22
5:5	10.50	11.20	41.40	0.48	0.51
2:8	6.30	24.30	55.10	0.20	0.79
0:10	0.00	28.00	57.20	0.00	1.00

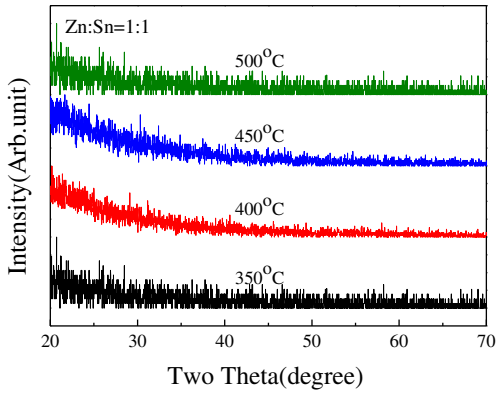

Fig. 2 XRD patterns obtained from the ZTO films at 350, 400, 450 and 500 °C annealing in air (Sn/(Zn:Sn)=1)

However, the TG/DSC in Fig. 1 suggested that the metal chlorines needed to be higher decomposing temperature (above 300 °C).

In order to confirm the decomposition of the organic groups, the AES depth profile of the ZTO film (annealed at 350 °C for 1 h at Sn/(Zn+Sn)=1) is shown in Fig. 1(b). The composition of the film was distributed uniformly in depth and there are no critical organic impurities (carbon and chlorine) in the ZTO film. It implies that solvent and organic molecules residues can't play roles to be obstacles for charge carrier accumulation and transportation in the conduction band even at 350 °C process. Also, the elemental compositions of different ZTO films are summarized in Table 1. As shown in Table 1, the relative ratio of Sn/(Zn+Sn) was controlled to 0, 0.2, 0.5, 0.8 and 1 as Sn concentration increased. Thus, the composition ratios are well-defined in ZTO solution, suggesting that the benefit of solution-process is manipulating various elements easily even under multi-composition materials.

Figure 2 shows the X-ray diffraction patterns of the spin-coated ZTO thin films annealed at 350, 400, 450 and 500 °C for 1 h in air. Based on the previous interpretation for ZnO film, the diffraction patterns exhibited substantial c-axis-orientation has been reported for high temperature annealed solution-coated ZnO films as the grain growth tends to favor the low energy (002) surface [13]. However, XRD patterns revealed that the solution-processed ZTO films were amorphous phases regardless of chemical compositions, and the amorphous structure was maintained during annealing up to 500 °C.

Figure 3 shows the representative transfer characteristics of the TFTs with the ZTO active layers as functions of ratios of Zn: Sn (10:0, 8:2, 5:5, 2:8 and 0:10). The saturation mobility (μ_{sat}) and threshold voltage (V_{th}) in the saturation region (V_{DS}=10 V) were calculated by fitting a straight line to the plot of the square root of drain current (I_{DS}) versus gate voltage (V_{GS}), according to the expression for a field-effect transistor. The subthreshold gate swing (S) value was extracted from the linear part of the log (I_{DS}) vs. V_{GS} plot [14].

$$I_{DS} = \frac{\mu_{SAT} C_i W}{2L}(V_{GS} - V_{TH})^2,$$

$$S = \left[\frac{\mathrm{d}(\log_{10} I_{DS})}{\mathrm{d}V_{GS}}\right]^{-1}$$

Where is the capacitance of gate insulator per unit area (C_i).

By changing the ratio of Zn: Sn at 350 °C, the μ_{sat} of ZTO TFTs showed the parabolic behavior: The values of μ_{sat} are 0.2×10^{-3}, 0.10×10^{-2}, 3.41 and 0.01 $cm^2/V{\cdot}s$ depending on 10:0, 8:2, 5:5 and 2:8 of Zn:Sn, respectively. Interestingly, the value of S.S also exhibited the similar behavior, having the lowest point (0.38 V/decade) at Sn/(Zn+Sn)=1. This result is also well matched with that of vacuum processed ZTO TFTs, reporting that the mobility reached the maximum value (about 30 $cm^2/V.s$) at Sn/(Zn+Sn)=1 [15]. The best performance of ZTO TFTs was the μ_{sat} of 3.4 $cm^2/V{\cdot}s$, threshold voltage of

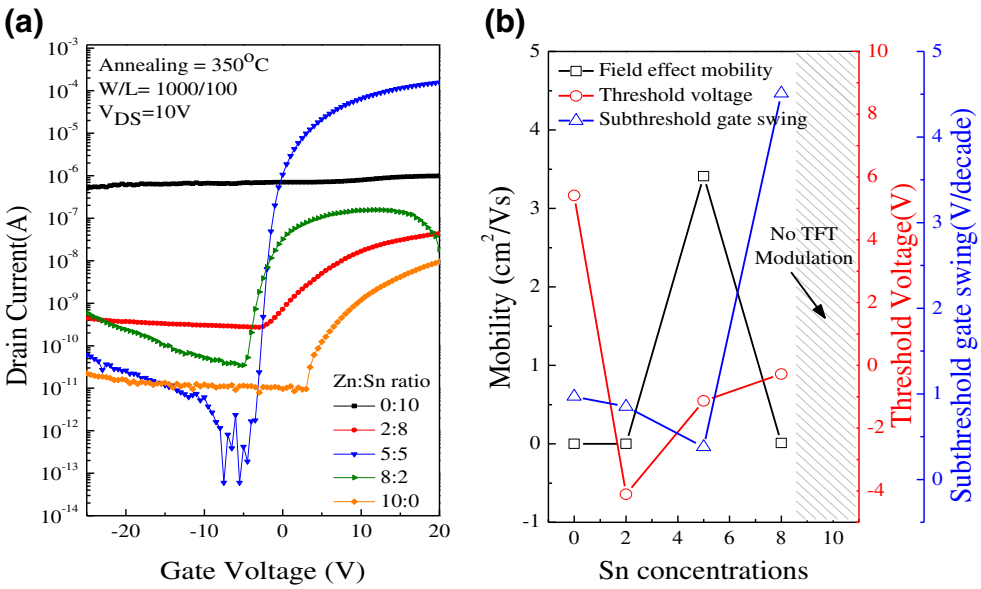

Fig. 3 (**a**) Representative transfer curves of ZTO TFTs on Sn/(Zn+Sn) ratio (Metal precursors: Zinc acetate dehydrate and Tin chloride dihydrate). (**b**) The electrical parameters of ZTO TFTs as a function of Sn/(Zn+Sn) ratio

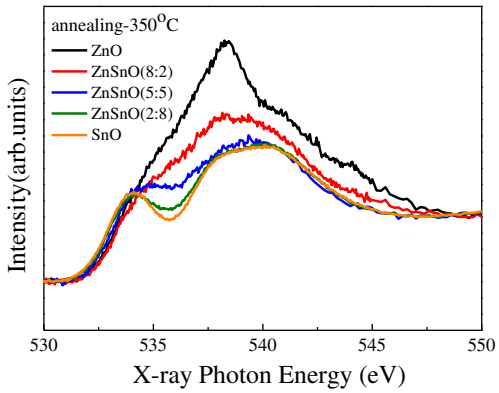

Fig. 4 O K edge XAS spectra of ZnSnO films as a function of Sn/(Zn+Sn) ratio

−1.1 V, on-to-off current ratios of 3.24×10^9, and subthreshold swings of 0.38 V/decade. However, the origin of parabolic behavior in ZTO TFTs is still unclear although a few groups already reported the tendency of ZTO TFTs under various methods [16]. In fact, charge transport in ZTO materials would be influenced by numerous factors such as the concentration of electrically-active defects, the structure ordering, and so on.

So, the XAS analysis of the O K1 edge was used to explain the films electronic structures related to changes in the conduction band and the molecular orbital ordering. The spectra were normalized in order to observe the relative changes of the molecular orbital structure in the conduction band. Normalizations of the XAS spectra were carefully performed by subtracting an x-ray beam background from the raw data and subsequently scaling the difference between pre- and post-edge levels to an arbitrary, but uniform, value. Through the normalizations of XAS spectra, the qualitative changes and comparison of conduction band features could be analyzed [17]. As shown Fig. 4, The normalized oxygen K1 edge spectra of ZnO are directly related to the oxygen p-projected states of the conduction band, which consists of unoccupied hybridization orbitals for Zn 4sp+O 2p. SnO causes the modification of the conduction band by incorporating SnO molecular structure near ~535 eV, attributed to oxygen 2p states hybridized with Sn 5 s and 5p states. The mixture of electronic structure between ZnO and SnO reduces the molecular orbital splitting of Zn 4p+O 2p from 535 to 540 eV, and divides the state of Sn 5 s+O 2p below ~535 eV. These changes of conduction band by the incorporation SnO into ZnO could enhance the conduction of charge transport because of the expansion of conduction band near the maximum of band gap and Fermi energy level. The XAS line-shapes of ZTO films could be associated mainly with the SnO_2. In other words, the slight splits mainly can see that reflect the changes of electrons structure due to Sn concentration in ZTO films.

On the other hand, in order to explain the parabolic behavior in detail, Sn*3d* peaks were obtained by XPS as a function of Sn content. The Fig. 5 showed the Sn*3d* spectra, separating into 2 peaks (Sn^{4+} and Sn^{2+}) using Gaussian fitting with the subtraction of a Shirley type background. The lower binding energy peak (Sn^{2+}) and higher binding energy peak (Sn^{4+}) are near 486.5 eV and 487.1 eV, respectively. Generally, the ZTO films could be converted into the various SnO-SnO_2 and ZnO-Zn phases. In particular, the phase of SnO-SnO_2 would be contributed to change of carrier concentration in terms of bond with metal and oxygen. The high oxidation state portion (Sn^{4+}) can increase the electron ($Sn^{2+}\rightarrow Sn^{4+}+2\,e$-) between SnO and SnO_2 phase, because Sn cation can allow for a dual valence which facilitates a reversible transformation Sn^{4+} (*n*-type) and Sn^{2+} (*p*-type) [18]. Very surprisingly, Sn^{4+} amounts in ZTO films drastically increase from 28.27 to 47.14 % by the peak point (Sn/(Zn+Sn)=1) and then, decreased rapidly below 20 %. This tendency could associate with the parabolic behavior of ZTO TFTs, suggesting that chemical states and amounts of Sn cation will be the key factor to control electrical performances of ZTO TFTs such as μ_{sat} and S.S.

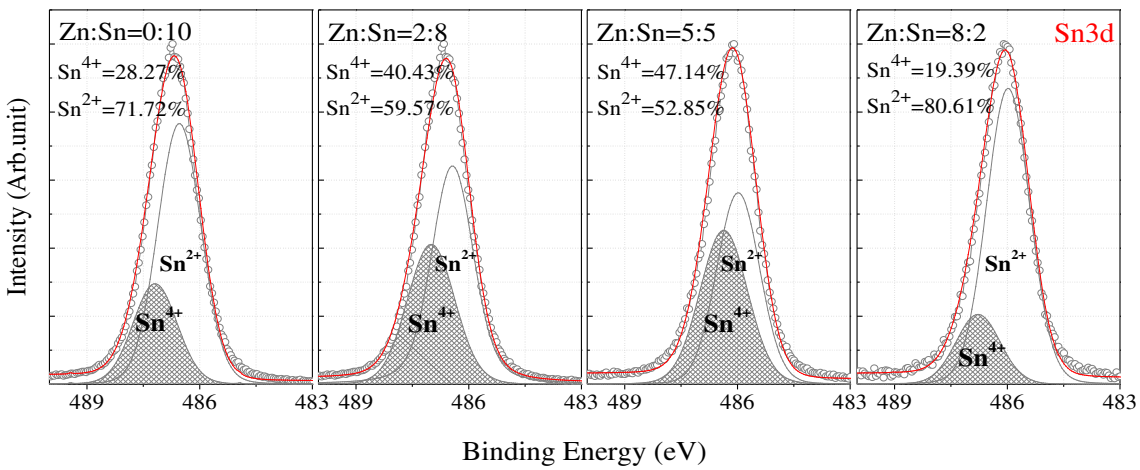

Fig. 5 Sn*3d* peaks of ZnSnO films as a function of Sn/(Zn+Sn) ratio

4 Conclusions

In summary, the ZTO films were fabricated by using the spin-coating process with combinatorial methods (Sn/(Zn+Sn)=0 ~1). The Zn and Sn precursor were thermal-decomposed completely after 350 °C annealing and All ZTO films didn't have any impurities such as C and Cl. Also, All ZTO films showed amorphous phases by 500 °C annealing temperature. As Sn/(Zn+Sn) ratio increased, the ZTO device performances (at 350 °C annealing in air) exhibited the parabolic behavior having best peak points of mobility (3.4 cm^2/V.s) and S.S (0.38 V/decade) at Sn/(Zn+Sn)=1. The change of conduction band by the incorporation SnO into ZnO may enhance electrical performances of ZTO TFTs. In addition, the parabolic behaviors of device parameters may mainly originate from the chemical state changes and total amount of Sn^{4+}/Sn^{2+} under various ZTO films.

Acknowledgments This work was partially supported by the IT R&D program of MKE/KEIT (Grant No. 10041416, The core technology development of light and space adaptable new mode display for energy saving on 7 in and 2 W) and partially supported by the MSIP under the ITRC support program (NIPA-2013-H0301-13-1004) supervised by the NIPA.

References

1. J.S. Park, W.-J. Maeng, H.-S. Kim, J.-S. Park, Thin Solid Films **520**, 1679–1693 (2012)
2. J.-S. Park, H. Kim, I.-D. Kim, J. Electroceram. (2013). doi:10.1007/s10832-013-9858-0
3. H. Yabuta, M. Sano, K. Abe, T. Aiba, T. Den, H. Kumomi, K. Nomura, T. Kamiya, H. Hosono, Appl. Phys. Lett. **89**, 112–123 (2006)
4. H.-S. Kim, J.-S. Park, J. Electroceram. (2013). doi:10.1007/s10832-013-9876-y
5. J.Y. Choi, S.S. Kim, S.Y. Lee, Appl. Phys. Lett. **100**, 022109 (2012)
6. C.Y. Koo, D. Kim, S. Jeong, C. Park, M. Jeon, W.-C. Sin, J. Jung, H.-J. Woo, S.-H. Kim, J. Ha, J. Moon, J. Korean Phys. Soc. **53**(1), 218–222 (2008)
7. D.-H. Lee, Y.-J. Chang, G.S. Herman, C.-H. Chang, Adv. Mater. **19**, 843–847 (2007)
8. D.H. Cho, S.H. Ko Park, S.H. Yang, C.W. Byun, K.I. Cho, M.K. Ryu, S.M. Chung, W.S. Cheong, S.M. Yoon, C.S. Hwang, J. Inf. Display **10**, 137 (2009)
9. W.J. Park, H.S. Shin, B. Du Ahn, G.H. Kim, S.M. Lee, K.H. Kim, H.J. Kim, Appl. Phys. Lett. **93**, 083508 (2008)
10. S.-J. Seo, C.G. Choi, Y.H. Hwang, B.-S. Bae, J. Phys. D. Appl. Phys. **42**, 035106 (2009). 5pp
11. K. Song, D. Kim, X.-S. Li, T. Jun, Y. Jeong, J. Moon, J. Mater. Chem. **19**, 8881–8886 (2009)
12. S. Jeong, Y. Jeong, J. Moon, J. Phys. Chem. C **112**(30), 11082–11085 (2008)
13. P. O'Brien, T. Saeed, J. Knowled, J. Mater. Chem. **6**(7), 1135–1139 (1996)
14. K. Song, Y. Jeong, T. Jun, C.Y. Koo, D. Kim, K. Woo, A. Kim, J. Noh, S. Cho, J. Moon, Jpn. J. Appl. Phys. **49**, 05EB02 (2010)
15. R.L. Hoffman, Solid State Electron **50**, 784–787 (2006)
16. M.G. McDowell, R.J. Sanderson, I.G. Hill, Appl. Phys. Lett. **92**, 013502 (2008)
17. K.B. Chung, J.P. Long, H. Seo, G. Lucovsky, D. Nordlund, J. Appl. Phys. **106**, 074102 (2009)
18. H. Yabuta, N. Kaji, R. Hayashi, H. Kumomi, K. Nomura, T. Kamiya, M. Hirano, H. Hosono, Appl. Phys. Lett. **97**, 072111 (2010)